Journal of Nuclear Materials 448 (2014) 436–440

Contents lists available at ScienceDirect

Journal of Nuclear Materials

journal homepage: www.elsevier.com/locate/jnucmat

Post-quench ductility evaluation of Zircaloy-4 and select iron alloys under design basis and extended LOCA conditions ☆

Y. Yan *, J.R. Keiser, K.A. Terrani, G.L. Bell, L.L. Snead

Oak Ridge National Laboratory, TN 37831, United States

ARTICLE INFO

Article history:
Available online 21 June 2013

ABSTRACT

Oxidation experiments were conducted at 1200 °C in flowing steam with tubing specimens of Zircaloy-4, 317, 347 stainless steels, and the commercial FeCrAl alloy APMT. The purpose was to determine the oxidation behavior and post-quench ductility under postulated and extended LOCA conditions. The parabolic rate constant for Zircaloy-4 tubing samples at 1200 °C was determined to be $k = 2.173 \times 10^7$ $g^2/cm^4/s$, in excellent agreement with the Cathcart–Pawel correlation. The APMT alloy experienced the slowest oxidation rate among all materials examined in this work. The ductility of post-quenched samples was evaluated by ring compression tests at 135 °C. For Zircaloy-4, the ductile to brittle transition occurs at an equivalent cladding reacted (ECR) of 19.3%. SS-347 was still ductile after being oxidized for 2400 s (CP–ECR ≈ 50%), but the maximum load was reduced significantly owing to the metal layer thickness reduction. No ductility decrease was observed for the post-quenched APMT samples oxidized up to 4 h.

Published by Elsevier B.V.

1. Introduction

Fuel rod cladding is the first barrier for retention of fission products in light water reactor (LWR) cores where the structural integrity of the cladding ensures safe operation of the reactor and coolable core geometry. The Zr alloys have been used in LWRs for past decades primarily due to their low thermal neutron cross-section. The main areas of research and development for zirconium alloy cladding have been focused on decreasing the waterside corrosion rate and hydrogen pick-up under normal operating conditions to increase the operational economy and safety margin [1,2]. The high-temperature steam oxidation behavior of zirconium alloy cladding under design basis loss of coolant accidents (LOCA) and over a broader set of conditions has been studied extensively in the past and has been found to be independent of minor alloying elements [3–11]. The recent earthquake and tsunami that overwhelmed the Fukushima plants, where three of the cores essentially experienced beyond design basis accidents, resulted in partial core meltdowns. The exposure of zirconium alloy cladding to high temperature steam resulted in production of a significant amount of heat and hydrogen gas that exacerbated the accident resulting in a more rapid pressure build-up in the containment, hydrogen explosion, and fission product release.

One approach for improving the safety margins during accident scenarios is to replace the current zirconium alloy cladding with iron based alloys that offer slower steam oxidation kinetics. A detailed discussion on the motivations and considerations upon adopting such an approach is offered in a companion paper in this journal [12]. Separately, the results from a broad study mapping the oxidation behavior of a wide range of iron alloys and comparing them to the benchmark case of zirconium alloys have also been provided [13,14]. In this work, a series of two-sided steam oxidation tests have been conducted on tubing specimens of Zircaloy-4 and select iron-based alloys at high temperature (1200 °C), followed by ring compression testing (RCT). In this manner, candidate iron-based alloy cladding materials with low steam oxidation rates and low ductility loss under design basis LOCA conditions, when compared to zirconium alloys, have been identified and examined side-by-side. As the Equivalent Cladding Reacted (ECR) is used for the current LOCA licensing criteria (10 CFR50.46) on the Zr alloys, we use ECR for other materials in order to compare their oxidation behavior to Zircaloy-4.

☆ This document was prepared as an account of work sponsored by an agency of the United States Government. Neither the United States Government nor any agency thereof, nor any of their employees, makes any warranty, express or implied, or assumes any legal liability or responsibility for the accuracy, completeness, or usefulness of any information, apparatus, product, or process disclosed, or represents that its use would not infringe privately owned rights. Reference herein to any specific commercial product, process, or service by trade name, trademark, manufacturer, or otherwise, does not necessarily constitute or imply its endorsement, recommendation, or favoring by the United States Government or any agency thereof. The views and opinions of authors expressed herein do not necessarily state or reflect those of the United States Government or any agency thereof.

* Corresponding author. Address: Fusion and Materials for Nuclear System Division, Oak Ridge National Laboratory, Mail Stop 6295, Building 3525, Room 103, Oak Ridge, TN 37831, United States. Tel.: +1 (865) 5749278.

E-mail address: yany@ornl.gov (Y. Yan).

0022-3115/$ - see front matter Published by Elsevier B.V.
http://dx.doi.org/10.1016/j.jnucmat.2013.05.071

Table 1
Alloy compositions in percent mass fraction.

Alloy	Fe	Zr	Ni	Cr	Al	Mo	Mn	Si	C	O	Other
Zircaloy-4	0.22	98.2	–	0.11	–	–	–	0.01	0.016	0.118	1.27Sn
317L SS	64.2	–	11.86	18.9	–	3.13	0.62	0.38	0.023	0.006	
347 SS	68.9	–	9.97	17.5	–	0.16	1.8	0.66	0.04	0.007	
APMT	69	0.1	0.12	21.6	4.93	2.77	0.1	0.53	0.03	0.049	0.12Y,0.16Hf

Note: These data were analyzed compositions by combustion methods.

2. Experimental procedure

The materials tested for this work were Zircaloy-4, Stainless Steel (SS)-317L, SS-347, and APMT alloy; a commercial oxide dispersion strengthened (ODS) FeCrAl alloy. The composition of the various alloys is provided in Table 1. The APMT tubing specimens were prepared from the iron-based alloy rods by drilling out the center. Specimen dimensions of all samples tested in this work were those characteristic of a 17 × 17 PWR fuel rod array: outer diameter (OD) of ≈9.50 mm and wall thickness of ≈0.57 mm. Test specimens were 25.00 mm long. Before the oxidation test, the diameter of each sample was measured with a caliper to an accuracy of ±0.03 mm. Sample weight measurements were conducted before and after each test using a balance with an accuracy of ±0.0001 g.

A 121.9 cm long resistance furnace was used for the steam oxidation test. The test chamber consisted of a quartz tube containing the sample and the flowing steam. Steam, at near-atmospheric pressure, flowed through the quartz-tube with a mass flux of 5.2 ± 0.5 mg/cm^2/s. A thermal benchmark test was conducted at 1200 °C in flowing steam using a monitor Type-S thermocouple strapped to the sample and the alumina sample-holding boat. The ramp times to reach the hold temperature are short compared to the hold times at these temperatures. The average cooling rate from the hold temperature to the 800 °C quench temperature was ≈12 ± 2 °C/s. The temperature–time curves were used to calculate the Cathcart–Pawel (CP) predicted weight gain (WG) and equivalent cladding reacted values [4].

After oxidation, 8 mm rings were sectioned from the oxidized samples for the RCT to evaluate the post-quench ductility. The samples were compressed radially using an Instron 6589 at a crosshead speed of 0.033 mm/s. Load–displacement data were recorded by the companion software. Tests were conducted at 135 °C by heating inside a furnace.

3. Results

3.1. Oxidation behavior

Fig. 1 shows the temperature histories for the three tests with Zircaloy-4 at 1200 °C used for baseline data. The plots represent the recording of the type-S monitor thermocouple. The uncertainty in this thermocouples about 2 °C when compared to a NIST calibrated type-S thermocouple at the maximum oxidation temperature (1200 °C). The onset of the high-temperature hold (Δt = 31, 303, and 872 s) is set 60 s after the samples being ramped to the pre-heat temperature by insertion into a preheated furnace. In addition to these plots, more tests were conducted for longer times (up to 14,400 s).

The oxidation times were determined using the Cathcart–Pawel (CP) equation described in Ref. [4]. This weight gain model was integrated over the actual temperature history, including the ramp, to generate a best-estimate model prediction of the weight gain during tests [5]. The model was again used to determine the time at the steady temperature to generate the same weight gain as was calculated for the actual temperature history.

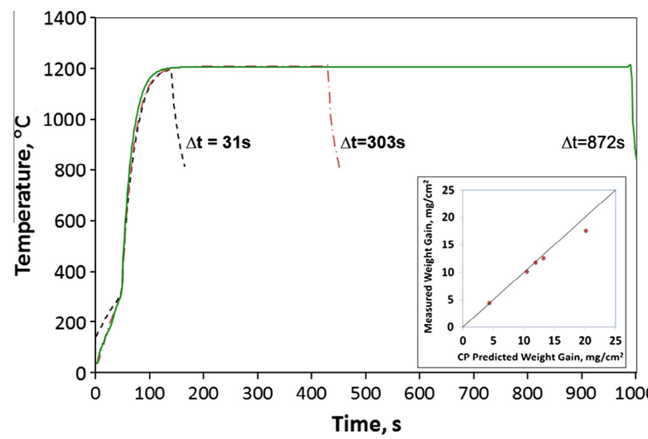

Fig. 1. Summary of the temperature histories for the steam oxidation tests for the hold time 31, 303, and 872 s at 1200 °C.

Table 2 is a summary of measured weight gain and ring compression results for oxidized Zircaloy-4 and others alloys tested for different times. The sample weight gains determined from the total change in sample weight before and after the test. The Zircaloy-4 cladding samples were oxidized at 1200 °C for times having CP calculated ECR up to 41%, and the other alloy samples were oxidized for longer times. It was found that some oxide layer flaked off SS-347 oxidized for 2400 s and SS-317 for 7200 s. The measured weight gain for Zircaloy-4 samples is in good agreement with the CP-predicted weight gain, as shown in the inset of Fig. 1. For isothermal oxidation at 1200 °C, the parabolic rate constant determined by the measured weight gain, $k = 2.173 \times 10^7$ (g/cm^2)^2/s, in excellent agreement with CP-coefficient $k = 2.185 \times 10^7$ (g/cm^2)^2/s [4].

From a comparison of the weight gain of tested samples (see Fig. 2), SS-317 and APMT showed much better oxidation resistance than Zircaloy-4 and SS-347 under the 1200 °C steam environment. In particular, the oxidation rate of APMT was extremely low. For the samples tested for 1600s, the weight gains of SS-317 and APMT were 3.6 mg/cm^2 and 10.3 × 10^{-2} mg/cm^2 respectively, compared to 24.7 mg/cm^2 for Zircaloy-4. Recent studies indicate that a slow-growing alumina surface oxide forms during the steam oxidation of the APMT [13–15], which shows promise for the highest temperature accident conditions for a nuclear reactor core. However, more extensive evaluation of its properties is needed, considering the other properties that affect in-reactor materials performance.

3.2. Post-quench ductility

Following the oxidation tests, ring compression tests were performed at 135 °C to evaluate the ductility of the oxidized samples [7,16]. A uniaxial compression of the samples yielded load–displacement curves which were analyzed by the traditional offset-displacement method used in analyzing tensile-test data. The offset displacement, determined from load–displacement data, was

Table 2
Sample weight gain measurements and ring compression test results for samples oxidized at 1200 °C and Quenched at 800 °C.

Materials	Target hold time (s)	Measured WG (mg/cm^2)	CP–WG (mg/cm^2)	Measured ECR (%)	CP–ECR (%)	Measured sample OD (mm)	Offset hoop strain (%)	Permanent hoop strain (%)
Zircaloy-4	31	4.41	4.33	7	7	9.50		
Zircaloy-4	233	10.13	10.52	16	16	9.50	3.8	1.6
Zircaloy-4	303	11.75	11.94	18	18	9.49	3.1	1.0
Zircaloy-4	378	12.53	13.23	19	20	9.49	2.5	0.8
Zircaloy-4	872	17.59	20.17	27	31	9.49	0.5	0.4
Zircaloy-4	1600	24.66	26.62	38	41	9.49	–	–
SS 317	303	1.27	11.94	2	18	9.50	>35	–
SS 317	872	2.16	20.17	3	31	9.50	>35	–
SS 317	1600	3.60	26.62	6	41	9.50	>35	–
SS 317	2400	4.56	32.46	7	–	9.50	>35	–
SS-317	7200	3.53[a]	–	–	–	9.51	>35	–
SS 347	303	5.23	11.94	8	18	9.50	>34	–
SS 347	872	24.4	20.17	38	31	9.53	>34	–
SS 347	1600	38.5	26.62	59	41	9.50	19	–
SS 347	2400	48.2[a]	32.46	–	–	9.50	8.4	–
APMT	378	8.9×10^{-2}	11.94	14×10^{-2}	18	9.51	>35	–
APMT	872	10.3×10^{-2}	20.17	16×10^{-2}	31	9.51	>35	–
APMT	1600	10.3×10^{-2}	26.62	16×10^{-2}	41	9.47	>35	–
APMT	2400	13.7×10^{-2}	32.46	21×10^{-2}	–	9.48	>35	–
APMT	7200	12.4×10^{-2}	–	–	–	9.49	>35	–
APMT	14,400	11.0×10^{-2}	–	–	–	9.49	>35	–

[a] Some oxide layer flaked off.

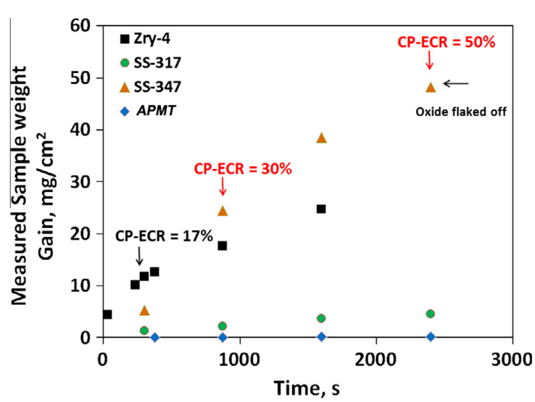

Fig. 2. Oxidation kinetics at 1200 °C in accordance with the measured sample weight gain at 1200 °C.

normalized to the as-fabricated outer diameter (9.50 mm) to give a nominal plastic hoop strain. Testing was stopped when a considerable load drop was seen, which was taken as an indication of cracking. The post-test diameters along and normal to the loading direction were measured directly and compared to the pre-test diameter to give a direct measure of permanent strain.

Fig. 3 shows the RCT results for Zircaloy-4 (Fig. 3a), SS-347 (Fig. 3b), and APMT (Fig. 3c). For ease of comparison, multiple load–displacement curves are placed on a single graph for different alloys. The curves are shifted along the *x*-axis but reflect the maximum load and change in displacement. For Zircaloy-4, displacement and maximum load clearly decrease as the ECR increases. Based on the criterion that standard offset strains >2% imply ductility [7], the Zircaloy-4 oxidized at 1200 °C is still ductile for ECR ≈ 19.3% (t = 378 s), but the offset strain of the sample oxidized for 872 s was reduced to about 0.5% (Table 2 and Fig. 3a), indicating that the sample became completely brittle when exposed to the steam (in just under 15 min). Metallography was performed on Zircaloy-4 samples oxidized at 1200 °C. High magnification micrographs at the eight circumferential locations confirmed uniform oxide layer thicknesses on both the outer surface and inner surface. The oxide layer thicknesses were measured and were in excellent agreement with the CP-calculation of the steam oxidation for Zircaloy-4 [4].

The plots for SS-347 clearly demonstrate the reduction in ductility that accompanies longer oxidation times (Fig. 3b). However, the offset strain of the SS-347 sample oxidized for 2400 s was still ⩾8.4%, indicating the sample still remained ductile. In addition the maximum loads of the RCT for SS-347 were significantly reduced when the oxidation time increased. Metallography was performed on all SS-347 samples oxidized at 1200 °C. The measurements indicated that the metal layer thicknesses for the samples oxidized for 303, 872, 1600 and 2400 s were reduced to 427, 286, 156 and 76 μm respectively, which is consistent with the maximum load decreasing shown in Fig. 3b. The inset of Fig. 3b shows a micrograph of the SS-347 oxidized for 2400 s. It appears that the metal layer sandwiched by the oxide layers remains ductile for the oxidized SS-347. This is the case since while zirconium exhibits an exceptionally large solubility for oxygen [17], oxygen solubility in ferritic and austenitic iron alloys is exceptionally low [18]. Consequently the drastic changes in mechanical properties of the remaining metal layer that occur in zirconium alloys as a result of oxygen uptake during steam oxidation are absent for Fe alloys. Similar observations have been made in the past on 304L tubing specimens oxidized in steam [19].

Fig. 3c show that there was very little change for the RCT results for APMT samples steam-oxidized at 1200 °C for up to 4 h, which is well beyond the design basis LOCA test conditions. The shapes of the plots almost remained the same, and no ductility reduction was observed for any of the oxidized APMT samples examined in this work. Fig. 3d shows a RCT comparison of APMT, SS-347 and Zircaloy-4 samples oxidized at 1200 °C for 872 s (equivalent to CP–ECR = 30%). Clearly, the APMT sample performs the best in the high temperature steam environment.

4. Conclusions

Post-quench ductility studies were conducted with Zircaloy-4, SS-317, SS-347, and APMT cladding samples at temperatures of 1200 °C, followed by cooling to 800 °C and then a water quench at room temperature for the purpose of determining the weight-gain coefficient and determining ductility under two-sided clad-

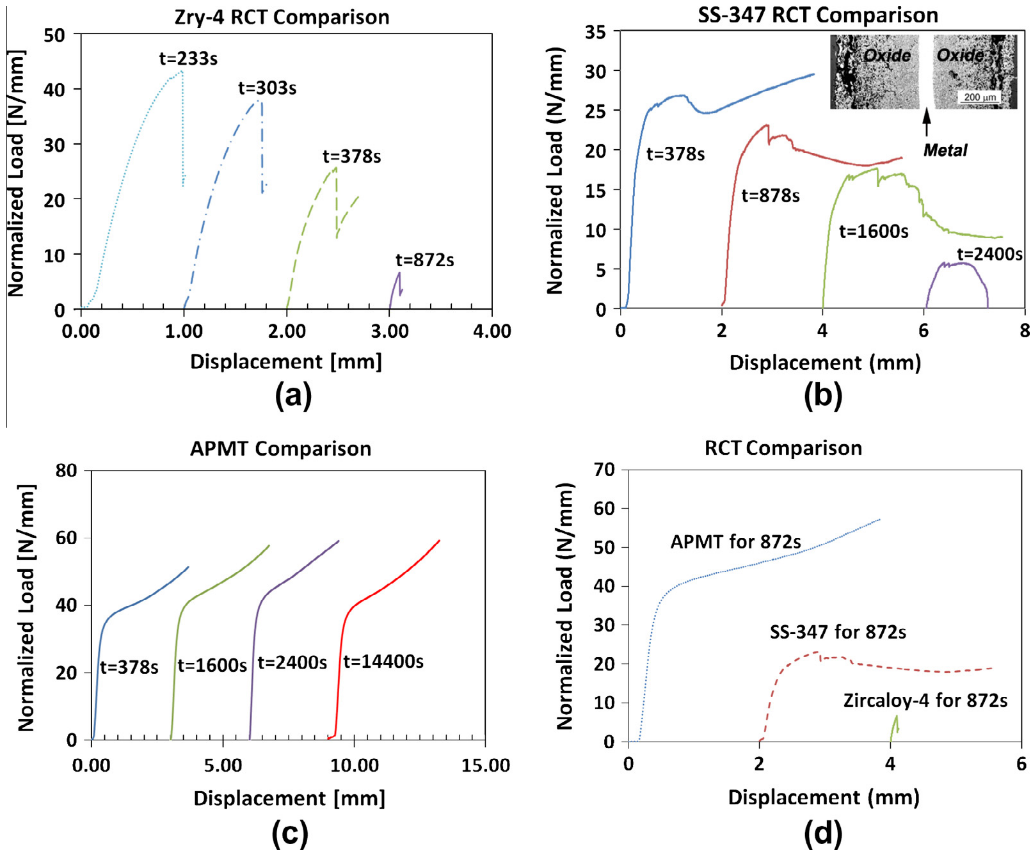

Fig. 3. Ring-compression load–displacement data for (a) Zircaloy-4 oxidized to 872 s, (b) SS-347 oxidized to 2400 s, (c) APMT oxidized to 14,400 s, and (d) comparison of Zircaloy-4, SS-347 and APMT oxidized to 872 s.

ding steam exposure to simulate the design basis LOCA conditions and beyond. The following conclusions were drawn from the results:

(1) Two-sided oxidation studies have been conducted on 17×17 Zircaloy-4 cladding exposed to steam at 1200 °C for hold times ranging from approximately 30 to 1600 s. The results from the tests have been analyzed and compared to the CP correlation predictions for weight gain. The parabolic rate constant is in excellent agreement with the CP model predictions. The weight-gain coefficient at 1200 °C determined by the measured weight gain is $k = 2.173 \times 10^7\ (g/cm^2)^2/s$.
(2) Other candidate cladding materials, such as SS-317, SS-347, and APMT were oxidized under the same test conditions as the Zircaloy cladding, but for much longer times that were well beyond design basis LOCA conditions. The APMT sample showed the slowest oxidation rate among all materials examined in this work; its oxygen pickup was very small for the test time up to 4 h at 1200 °C.
(3) The ductility of post-quenched samples was evaluated by RCT. Generally speaking, the displacements and maximum loads gradually decrease for Zircaloy-4 and SS-347 as the oxygen pickup increases as a result of the increase in test time. For Zircaloy-4, the ductile to brittle transition ECR is about ≈19.3%. SS-347 was still ductile after being oxidized for 2400 s (CP–ECR ≈ 50%), but the maximum load was reduced significantly due to the metal layer thickness reduction.SS-317 does not show a ductility decrease for the samples tested up to 7200 s. No ductility decrease was observed for the post-quenched APMT samples oxidized up to 4 h.
(4) This work was mainly focused on the material performance under proscribed accident conditions. It is widely accepted that the selection of future candidate materials should consider the other properties that affect in-reactor materials performance as well, such as the neutron absorption cross section, thermal conductivity, thermal expansion, melting point, phase transformation behavior, corrosion resistance, and high-temperature oxidation rate. More studies on the cladding candidate materials are under way, the results of which will be reported in the near future.

References

[1] A.M. Garde, R.J. Garde, G. Pan, R. Baranwal, L. Hallstadius, T. Cook, F. Carrera, advanced zirconium alloy for PWR application, J. ASTM Intl. 7(9). http://dx.doi.org/10.1520/JAI103030.
[2] V. Chabretou, P.B. Hoffmann, S. Trapp-Pritsching, G. Garner, P. Barberis, V. Rebeyrolle, J.J. Vermoyal, Ultra low tin quaternary alloys PWR performance-impact of tin content on corrosion resistance, irradiation growth, and mechanical properties, J. ASTM Int. 8(5). http://dx.doi.org/10.1520/JAI103013.
[3] L. Baker, L.C. Just, Studies of Metal–Water Reactions at High Temperatures: III. Experimental and Theoretical Studies of the Zirconium–Water Reaction, ANL-6548, May 1962.
[4] J.V. Cathcart, R.E. Pawel, R.A. McKee, R.E. Druschel, G.J. Yurek, J.J. Cambell, S.H. Jury, Zirconium Metal–Water Oxidation Kinetics IV Reaction Rate Studies, ORNL/NUREG-17, August 1977.
[5] Y. Yan, R.V. Strain, T.S. Bray, M.C. Billone, High Temperature Oxidation of Irradiated Limerick BWR Cladding, NUREG/CP-0176 May 2002 pp. 353–372.
[6] F. Nagase, T. Otomo, H. Uetsuka, Nucl. Sci. Technol. 40 (2003) 213–219.
[7] M. Billone, Y. Yan, T. Burtseva, R. Daum, Cladding Embrittlement during Postulated Loss-of-Coolant Accidents, NUREG/CR-6967, ANL-07/04, July 2008.
[8] J.-P. Mardon, D. Charquet, J. Senevat, Influence of composition and fabrication process on out-of-pile and in-pile properties of M5 alloy, in: G.P. Sabol, G.D. Moan (Eds.), Zirconium in the Nuclear Industry: 12th International Symposium, ASTM STP 1354, American Society for Testing and Materials, West Conshohocken, PA, 2000, pp. 505–524.

[9] R.J. Comstock, G. Schoenberger, G.P. Sabol, Influence of processing variables and alloy chemistry on the corrosion behavior of ZIRLO nuclear fuel cladding, in: E.R. Bradley, G.P. Sabol (Eds.), Zirconium in the Nuclear Industry: 11th International Symposium, ASTM STP 1295, American Society for Testing and Materials, 1996, pp. 710–725.
[10] J.C. Brachet, L. Portier, J. Hivroz, D. Hamon, T. Guilbert, T. Bedel, P. Yvon, J.P. Mardon, P. Jacques, Influence of hydrogen content on the α/β phase transformation temperature and on the thermal–mechanical behavior of Zy-4, M4 (ZrSnFeV), and M5™ (ZrNbO) alloys during the first phase of LOCA transient, in: G.D. Moan, P. Rudling (Eds.), Zirconium in the Nuclear Industry, ASTM STP 1423, American Society for Testing and Materials, 2002, pp. 673–701.
[11] Y. Yan, T. Burtseva, M. Billone, J. Nucl. Mater. 393 (2009) 433–448.
[12] K.A. Terrani, S.J. Zinkle, L.L. Snead, J. Nucl. Mater. 448 (2014) 420–435, http://dx.doi.org/10.1016/j.jnucmat.2013.06.041.
[13] T. Cheng, J.R. Keiser, M.P. Brady, K.A. Terrani, B.A. Pint, J. Nucl. Mater. 427 (1–3) (2012) 396–400.
[14] B.A. Pint, K.A. Terrani, M.P. Brady, T. Cheng, J.R. Keiser, J. Nucl. Mater. 440 (2013) 420–427.
[15] D.J. Young, D. Naumenko*, L. Niewolak, E. Wessel, L. Singheiser, W.J. Quadakkers, Mater. Corros. 10 (2010) 61.
[16] Y. Yan, T.A. Burtseva, M.C. Billone, Post-quench Ductility Results for North Anna Highburnup 17×17 ZIRLO Cladding with Intermediate Hydrogen Content, ANL Letter Report to NRC, April 17, 2009. ML091200702: <http://www.nrc.gov/reading-rm/adams.html>.
[17] J.P. Abriata, J. Garcés, R. Versaci, J. Phase Equilib. 7 (2) (1986) 116–124.
[18] J.L. Meijering, Acta Metall. 3 (1955).
[19] L. Portier, J.C. Brachet, V. Vandenberghe, T. Guilbert, V. Lezaud-Chaillioux, C. Bernard, V. Rabeau, Fontevraud 7 (2010) (Paper Reference No. A027).